Available online at www.sciencedirect.com

SciVerse ScienceDirect

Scripta Materialia 66 (2012) 190–193

Scripta MATERIALIA

www.elsevier.com/locate/scriptamat

Interrelationship between grain size-induced and strain-induced broadening of X-ray diffraction profiles: What we can learn about nanostructured materials?

E. Zolotoyabko,[a,*] J.L.M. Rupp[b] and L.J. Gauckler[c]

[a]*Department of Materials Engineering, Technion-Israel Institute of Technology, Haifa 32000, Israel*
[b]*Department of Materials Science and Engineering and Department of Nuclear Science and Engineering, Massachusetts Institute of Technology (MIT), Cambridge, MA 02139, USA*
[c]*Department of Materials, ETH Zurich, Wolfgang-Pauli-Str. 10, CH-8093 Zurich, Switzerland*

Received 16 August 2011; revised 23 October 2011; accepted 24 October 2011
Available online 29 October 2011

The two main mechanisms that cause the broadening of X-ray diffraction profiles in polycrystalline materials, i.e. those due to finite grain size and local strain inhomogeneities, are usually considered independently. In this paper, we discuss the potential interrelationship between them and propose a phenomenological equation which links the dispersion of strain distribution to grain size via the width of distorted regions near grain boundaries and the lattice disorder therein. The developed approach is applied to characterize crystallization processes in Gd-doped ceria films.

Keywords: X-ray diffraction; Grain boundaries; Crystallization; Nanostructure; Ceramic thin films

One of the classical applications of X-ray diffraction to materials science is the measurement of the average grain size, L, and the parameters of spatial strain distribution, thus characterizing the microstructure of polycrystalline materials (see e.g. Ref. [1]). More accurately, X-ray diffraction provides information on the size of crystalline blocks, which coherently scatter X-rays. For the sake of convenience, we will use the term "grain size" in this sense throughout this paper. Note that for nanostructured materials both terms practically coincide.

Strains in materials, in general, are the result of mechanical deformation. It is worth noting that inhomogeneous strain fields can also exist without the application of external force. In this case, local strains originate from lattice defects and their interactions. As was shown in the pioneering works of Krivoglaz (see Ref. [2] and references therein), inhomogeneous strain fields, produced by various defects, strongly influence X-ray diffraction profiles. In practical terms, the measured effect is always averaged over the sample volume from which the X-ray diffraction intensity is taken. Two important average parameters are usually considered: mean strain value (i.e. the first moment of the strain distribution), which causes the shift of the diffraction peak position, and mean square root value (i.e. the second moment or dispersion, σ, of the strain distribution), which results in the diffraction peak broadening. The latter is the focus of this study.

Two sources of peak broadening, i.e. those due to finite grain size, L, and dispersion, σ, of strain distribution, are regularly considered independently. There are few approaches for separating and extracting these particular effects from the measured widths of X-ray diffraction profiles. The most widely accepted routes are based on the classical Williamson–Hall or Warren–Averbach algorithms (see e.g. Ref. [1]), corrected by the dislocation orientation factors [3]. Dislocation-induced anisotropic broadening of diffraction profiles along different directions in reciprocal space is considered in e.g. Refs. [4,5].

Another approach for extracting the parameters L and σ is based on approximating diffraction profiles by special functions (e.g. by Voigt function, as in Refs. [6,7]) or, more generally, on whole diffraction pattern modeling [8].

In this paper, we point out a potentially important quantitative interrelationship between the grain size, L,

* Corresponding author. E-mail: zloto@tx.technion.ac.il

1359-6462/$ - see front matter © 2011 Acta Materialia Inc. Published by Elsevier Ltd. All rights reserved.
doi:10.1016/j.scriptamat.2011.10.037

and the dispersion parameter, σ, which has not been investigated yet. This interrelationship is easily revealed by recalling the following qualitative considerations [6]. A virtually perfect crystal has no inhomogeneous strain fields. Grains, "visible" by X-ray diffraction, are almost perfect crystal blocks with a low dispersion parameter, δ_{cr}, due to a small amount of lattice defects within the grain interior. In contrast, distorted (i.e. partially disordered) crystal areas, such as grain boundaries and the adjacent regions inside grains, are characterized by much higher dispersion values, $\delta_b \gg \delta_{cr}$. For the sake of convenience, we will call parameter δ_b the disorder parameter and call the distorted areas "grain boundaries". Under the condition of a constant total volume, larger crystal blocks imply a reduced number of "grain boundaries", which results in lower integrated σ-values measured by X-ray diffraction. Statistical averaging over the irradiated volume of the sample allows us to express the dispersion, σ, via the volume fraction, Ω, of crystalline grains:

$$\sigma^2 = \Omega\delta_{cr}^2 + (1-\Omega)\delta_b^2 \quad (1)$$

In order to further develop Eq. (1) in terms of grain size, L, we build a simple three-dimensional model, in which the cube-shaped grains with dimensions $L \times L \times L$ are separated by "grain boundaries" of width H. Note that the grain boundary region, which affects the X-ray diffraction, is determined by the related strain fields and is always larger than a specific geometrical object. Considering the proportion between the crystal and grain boundary volume fractions in this model, we find that the dispersion, σ, measured by X-rays is related to the average grain size, L, as follows:

$$\sigma^2 = \chi^3\delta_{cr}^2 + (1-\chi^3)\delta_b^2 \quad (2)$$

with

$$\chi = L/(L+H) \quad (3)$$

According to Eq. (2), at constant parameters H, δ_b and δ_{cr}, the dispersion, σ, rapidly decreases with increasing grain size at $L \gg H$ (due to the diminution of the second term in Eq. (2)). This conclusion is consistent with recent molecular dynamic simulations for nanocrystalline Pd [9].

In this paper, we apply Eqs. (2) and (3) in order to fit experimental data for the grain size, L, and dispersion, σ, obtained with 20 mol.% Gd-doped CeO_2 (ceria) sprayed thin films [10,11], and in that way to better understand the time- and temperature-dependent crystallization processes in this material system. Gd-doped ceria is a promising ion conductor for solid electrolyte fuel cells. Numerous investigations of ceria and doped ceria compounds have shown enhanced ionic conductivity due to the high mobility of oxygen vacancies and phase transformations related to the reduction of the oxidation state of Ce ions [12], the dependence of the lattice parameter and electrical properties on grain size [13], and the complicated behavior of the lattice parameter with temperature due to interaction between cations and oxygen vacancies [14,15].

Our samples of Gd-doped CeO_2 were initially produced by spray pyrolysis as amorphous materials followed by crystallization at elevated temperatures. The grain growth in the nanocrystalline Gd-doped CeO_2 and non-doped CeO_2 (ceria) showed self-limited grain growth and relaxation of the dispersion, σ, with time until reaching the temperature-dependent constant levels [10,16]. The Williamson–Hall approach was used in order to separately extract the grain size, L, and dispersion, σ, as functions of annealing temperature and duration, from the measured widths of X-ray diffraction profiles. The experimental procedures are described in more detail in Refs. [10,11].

The most interesting finding of the above-mentioned research is the observation in Ref. [10] of self-limited grain growth with annealing time, t, at rather low annealing temperatures of 600–1000 °C:

$$L(t) = L_\infty + (L_0 - L_\infty)\cdot\exp(-t/\tau_L) \quad (4)$$

The parameters L_0 and L_∞ in Eq. (4) are the initial and final grain sizes, and τ_L is the temperature-dependent relaxation time. The measured dispersion, σ, exhibited analogous behavior:

$$\sigma(t) = \sigma_\infty(\sigma_0 - \sigma_\infty)\cdot\exp(-t/\tau_\sigma) \quad (5)$$

with characteristic relaxation time, τ_σ, which is also temperature dependent. Note that similar experimental results concerning time dependences of the parameters L and σ were obtained in a study of the grain growth kinetics of nanocrystalline iron [17].

In Refs. [10,11], self-limited grain growth of the Gd-doped ceria thin films was related to the non-complete crystallization of ceramic material (see also Refs. [16,18]). It was reported that the grain growth is accompanied by a considerable reduction of the dispersion, σ, within similar relaxation time spans. At annealing temperatures higher than 1000 °C, the classical parabolic grain growth law was observed [16]. Our analysis (below) generally confirms this picture, though showing it in more detail.

In practical terms, the measured values of grain size, $L(t)$, from Ref. [10] were used as an input to Eq. (2) in order to calculate the temporal dependences, $\sigma(t)$, at different annealing temperatures, T, and to compare them with experimental data, $\sigma(t)$, from Ref. [10]. We also assumed that the effective width of our "grain boundaries", H, and the disorder parameter, δ_b, within these grain boundaries exponentially attenuate with annealing time, i.e. obey the Debye relaxation:

$$P = A + B\,\exp(-t/\tau) \quad (6)$$

with characteristic relaxation times, τ. The parameters A, B and τ, are different for the width, H, and disorder parameter, δ_b. Therefore, a total of six (3×2) fitting parameters are varied until the best fit between experimental data and simulations based on Eq. (2) is achieved.

Calculated curves, $\sigma(t)$, were compared with experimental data collected at annealing temperatures 600, 700, 800 and 900 °C. The extracted "grain boundary" width, H, and the disorder parameter, δ_b, are plotted as functions of annealing time at different annealing temperatures in Figures 1 and 2, respectively. As expected, both parameters decrease substantially with annealing time and with increasing annealing

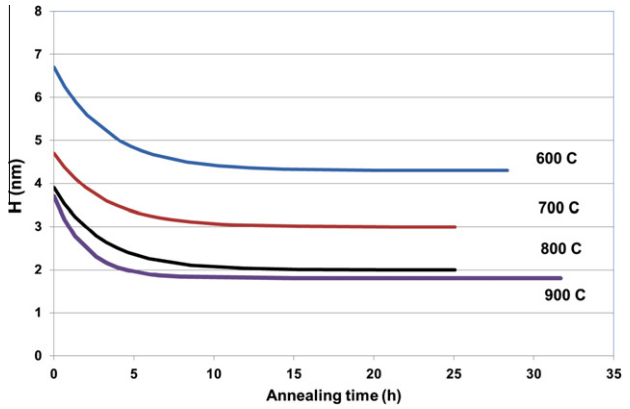

Figure 1. The "grain boundary" width, H, as a function of annealing time at different temperatures, extracted from the fitting of experimental data using Eqs. (2), (3), and (6).

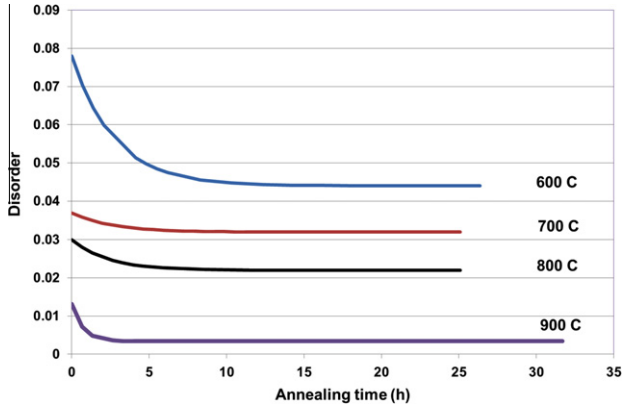

Figure 2. The disorder parameter, δ_b, as a function of annealing time at different temperatures, extracted from the fitting of experimental data using Eqs. (2), (3), and (6).

temperature. For example, prolonged annealing causes the disorder parameter to drop from $\delta_b = 0.078$ down to $\delta_b = 0.044$ at 600 °C, and from $\delta_b = 0.013$ down to $\delta_b = 0.0034$ at 900 °C (see Fig. 2). The width, H, decreases from 6.7 to 4.3 nm at 600 °C. Note that these values are not far away from the initial grain size, $L_o = 10$ nm, at this temperature [10]. At higher annealing temperatures, the width H becomes systematically smaller, varying from $H = 3.7$ nm down to $H = 1.8$ nm for an annealing temperature of 900 °C (see Fig. 1). It seems that the latter value of H is approaching the equilibrium "grain boundary" width in this polycrystalline sample. As already mentioned, the "grain boundary" width, H, probed by X-ray diffraction is the region where strain gradients are still significant, and hence the H-value is somewhat larger than the width of the grain boundary considered as a geometrical object.

Bearing in mind that relaxation times, τ, are defined by some energy barriers (activation energies) as:

$$\tau = \tau_0 \exp(\Delta E/kT) \tag{7}$$

one can find the respective activation energies, ΔE, by plotting (on a logarithmic scale) the values of τ as a function of the inverse absolute temperature ($1/T$).

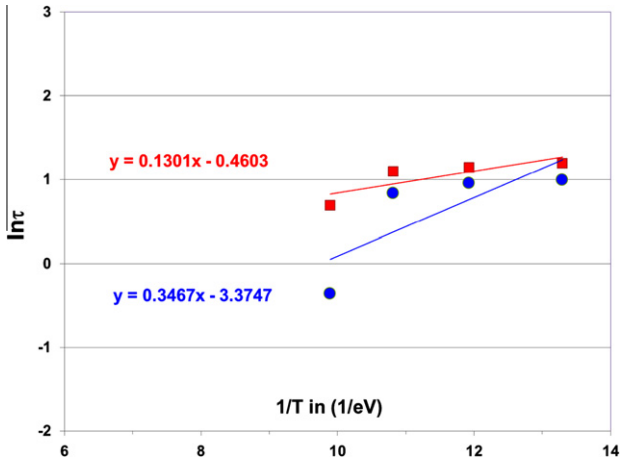

Figure 3. Relaxation times (on a logarithmic scale, $\ln(\tau)$) as a function of the inverse absolute temperature of annealing treatment (in eV^{-1}), extracted for "grain boundary" width, H (squares), and disorder parameter, δ_b (circles).

These plots for relaxation times extracted for the H and δ_b parameters are presented in Figure 3, in which, for the sake of convenience, absolute temperature is expressed in electron volts. Correspondingly, the activation energies displaced in Figure 3, i.e. the slopes of the linear trend lines, are also given in electron volts. We should mention the rather small values of ΔE of 0.13 and 0.35 eV for the kinetics of the width, H, and the disorder parameter, δ_b, respectively. These values are much lower than the activation energy of $E_a = 1.6$ eV measured for crystallization from the amorphous phase in this system [16,18]. This means that at relatively low temperatures, when the crystallization process is not yet complete, the grain growth will be limited by the presence of significant amounts of amorphous (and related highly disordered) regions remaining in the system. Atomic rearrangements in these regions are stopped at different levels, depending on the annealing temperature (as is clearly seen in Figs. 1 and 2). This is due to the high value of $E_a \gg \Delta E$. Put simply, atomic rearrangements are fast in crystallized regions containing grain boundaries and slow in highly disordered regions related to amorphous remnants, the latter seemingly being responsible for self-limited grain growth regime.

It is also known from Raman measurements that the ionic bonds in fully crystalline ceria films are weaker than those in high-temperature sintered bulk ceramics or amorphous ceria-based films. This can be deduced experimentally from the F_{2g} (1)O–Ce–O(1) stretching modes, which for fully crystalline bulk samples appear at lower wave-numbers than those in thin films [19]. Thus, it is important to note that the increased atomic rearrangements in the crystallized regions reported here occur at faster velocities than in partially disordered regions, but the thin film lattices remain at lower packing densities than in bulk ceramics. Recent time–temperature–transformation diagrams produced for the crystallization of ceria-based films also agree with the presented estimation of the energetically lower grain boundary kinetics compared to overall crystallization kinetics [18]. The crystallization rates of the films were

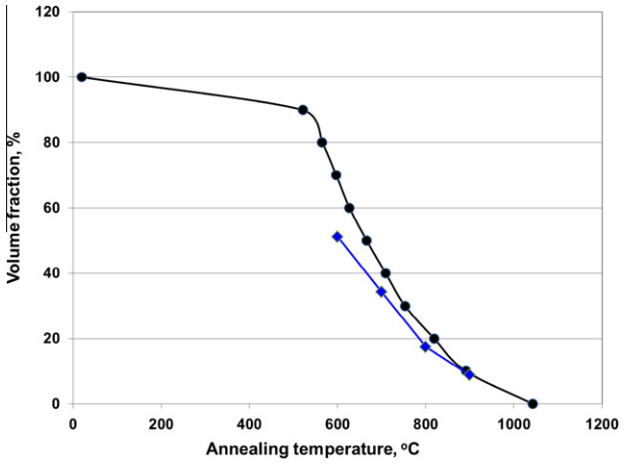

Figure 4. Total volume fractions of amorphous phase (circles) and "grain boundaries" (diamonds, Eq. (8)) as functions of annealing temperature.

increased by one order of magnitude once a critical amount of grains of overall 20% crystallinity were developed in the films' microstructure.

Supposing that the highly distorted/disordered regions mentioned above are related to the concentration of our grain boundaries, and thereby to the grain size, we can estimate their volume fraction, V_{gb}, as:

$$V_{gb} = 1 - \Omega = 1 - \chi^3 = 1 - [L/(L+H)]^3 \qquad (8)$$

(see Eqs. (1)–(3)). Taking the calculated equilibrium (i.e. at the limit of large annealing times, t) values of "grain boundary" widths, H, and the measured equilibrium grain sizes, L, and substituting them into Eq. (8), we find the volume fraction $V_{gb} = 1 - \Omega$ as a function of annealing temperature, T. The thus obtained $V_{gb}(T)$ plot is shown in Figure 4, together with the amorphous volume fraction, $V_a(T)$, measured by differential scanning calorimetry [11]. We see that the two curves exhibit similar behavior, at least at higher annealing temperatures, which confirms the assumption that most of the highly disordered phase is connected to our grain boundaries.

At temperatures higher than 900 °C, the amorphous phase completely disappears [10,11] and, as can be seen from Figures 1 and 2, "grain boundaries" are stabilized with a width down to $H = 1.8$ nm and the disorder parameter down to $\delta_b = 0.003$. The latter value is only three times larger than the dispersion parameter, $\delta_c = 0.001$, within crystalline grains at 900 °C, also extracted as a result of a fitting procedure. Such well organized and thin grain boundaries act as rather low energy barriers which can easily be overcome by diffusion, resulting in classical parabolic grain growth at temperatures higher than 1000 °C [10].

In summary, we found an interrelationship between such important microstructural parameters as grain size and the dispersion of spatial strain distribution and, on this basis, have developed a novel route for microstructural analysis in polycrystalline materials. Since we deal with volume fractions of perfect regions (grains) and distorted or disordered regions (like grain boundaries), the most important applications of this analysis are expected for nanostructured materials, e.g. thin metal oxide films. For example, applying our method to the crystallization kinetics of Gd-doped ceria allowed us to quantitatively explain the previously observed phenomenon, i.e. self-limited grain growth at low annealing temperatures. We found that the extracted activation energies for atomic rearrangements in the distorted crystalline regions (grain boundaries) are much lower (by nearly one order of magnitude) than the activation energy for the amorphous/crystalline phase transformation. This implies that atomic rearrangements are fast in the distorted crystalline regions related to grain boundaries and slow in the amorphous remnants, the latter possibly contributing to the stagnation of grain growth at rather low annealing temperatures.

E.Z. thanks the Shore Research Fund for partial financial support of this work. The Swiss National Science Foundation is acknowledged for the advanced researcher fellowship PA00P2-134153 for 2011/2012 awarded to J.R.

[1] B.E. Warren, X-ray Diffraction, Dover Publications, New York, 1990.
[2] M.A. Krivoglaz, X-Ray and Neutron Diffraction in Nonideal Crystals, Springer-Verlag, Heidelberg, 1996.
[3] T. Ungar, A. Boberly, Appl. Phys. Lett. 69 (1996) 3173–3175.
[4] R.I. Barabash, P. Klimanek, J. Appl. Crystallogr. 32 (1999) 1050–1059.
[5] R. Barabash, Mater. Sci. Eng. A 309–310 (2001) 49–54.
[6] E. Zolotoyabko, J.P. Quintana, J. Appl. Crystallogr. 35 (2002) 594–599.
[7] B. Pokroy, A.N. Fitch, E. Zolotoyabko, Crystal Growth Des. 7 (2007) 1580–1583.
[8] P. Scardi, M. Leoni, Acta Crystallogr. A 58 (2002) 190–200.
[9] A. Stukowski, J. Markmann, J. Weissmüller, K. Albe, Acta Mater. 57 (2009) 1648–1654.
[10] J.L.M. Rupp, A. Infortuna, L.J. Gauckler, Acta Mater. 54 (2006) 1721–1730.
[11] J.L.M. Rupp, C. Solenthaler, P. Gasser, U.P. Muecke, L.J. Gauckler, Acta Mater. 55 (2007) 3505–3512.
[12] I. Riess, R. Koerner, M. Ricken, J. Noelting, Solid State Ionics 28 (1988) 539–541.
[13] H.L. Tuller, Solid State Ionics 131 (2000) 143–157.
[14] A. Kossoy, Y. Feldman, R. Korobko, E. Wachtel, I. Lubomirsky, J. Maier, Adv. Funct. Mater. 19 (2009) 634–641.
[15] A. Kossoy, A.I. Frenkel, Q. Wang, E. Wachtel, I. Lubomirsky, Adv. Mater. 22 (2010) 1659–1662.
[16] J.L.M. Rupp, B. Scherrer, A. Harvey, L.J. Gauckler, Adv. Funct. Mater. 19 (2009) 2790–2799.
[17] H. Natter, M. Schmelzer, M.S. Loffler, C.E. Krill, A. Fitch, R. Hempelmann, J. Phys, Chem. B 104 (2000) 2467–2476.
[18] J.L.M. Rupp, B. Scherrer, N. Schäuble, L.J. Gauckler, Adv. Funct. Mater. 20 (2010) 2807–2814.
[19] J.L.M. Rupp, B. Scherrer, L.J. Gauckler, Phys. Chem. Chem. Phys. 12 (2010) 11114–11124.